Int. J. Heat Mass Transfer. Vol. 30, No. 7, pp. 1307–1318, 1987
Printed in Great Britain

0017–9310/87 $3.00 + 0.00

Experiments on mixed convection heat transfer for airflow in a horizontal and inclined channel

J. R. MAUGHAN and F. P. INCROPERA
Heat Transfer Laboratory, School of Mechanical Engineering, Purdue University, West Lafayette, IN 47907, U.S.A.

(*Received* 7 *August* 1986 *and in final form* 6 *November* 1986)

Abstract—Experiments have been performed to investigate mixed convection heat transfer in the thermal entry region of a parallel plate channel heated uniformly from below. The effect of surface heat flux and channel orientation on the local Nusselt number was studied for $Pr = 0.7$, $125 < Re < 500$, $7 \times 10^3 < Gr^* < 1 \times 10^6$, and $0 < \theta < 30°$. Heat transfer was initially dominated by forced convection and showed a rapid decline in the Nusselt number. Following the onset of thermal instability, secondary flow development caused a sharp increase in the Nusselt number, which was followed by a maximum and subsequent oscillations. The Nusselt number oscillations eventually decayed, yielding a fully developed value which depended on the Grashof number. The onset of instability was delayed by decreasing the Grashof number and/or by increasing the Reynolds number and the inclination angle. For the inclined channel, significant heat transfer enhancement occurred prior to onset of the secondary flow.

1. INTRODUCTION

BUOYANCY driven secondary flows can enhance forced convection heat transfer in compact heat exchangers, flat plate solar collectors, and in the cooling of electronic components and circuitry. Flow over a heated flat plate or through a parallel plate channel is common to each of these applications.

Early analyses of mixed convection on a heated horizontal plate [1, 2] considered perturbations of the two-dimensional boundary layer equations and predicted that buoyancy forces would increase heat transfer by inducing a favorable pressure gradient. As fluid passes along a heated surface, it becomes less dense, creating a small reduction in pressure which accelerates the flow and enhances heat transfer.

In most cases, the foregoing effect is small and, before it causes appreciable enhancement, unstable temperature gradients imposed by bottom heating initiate an ascending (secondary) flow of warm boundary layer fluid into the free stream. Investigations of the resulting three-dimensional flow [3, 4] revealed it to be an effective mechanism for heat transfer enhancement. Experiments, which were performed for water flow over an isothermal plate, revealed that onset of the thermal instability was followed by the formation of longitudinal vortices and a substantial increase in the heat transfer coefficient above the forced convection limit. Subsequent variations of the coefficient with the longitudinal coordinate decayed to a final value that was typical of turbulent free convection. Comparison of these results with the earlier analyses indicated that secondary motion begins before the streamwise pressure gradient can increase heat transfer by more than 1%.

Two-dimensional boundary layer analyses have also been performed for flow over an inclined plate [5, 6]. For an inclined surface, however, two mechanisms can enhance heat transfer prior to the onset of secondary flow. In addition to the induced streamwise pressure gradient, a component of the buoyancy force accelerates the flow directly. This effect is much stronger than that of the pressure gradient and appreciable enhancement can occur before the onset of instability. Although two-dimensional mixed convection on an inclined flat plate has been experimentally studied [6] and theoretical predictions of the onset of instability have been made [7], the subsequent three-dimensional secondary flow and the associated heat transfer enhancement have not been considered.

Mixed convection flow between horizontal parallel plates (or in a channel of large aspect ratio) initially attracted attention because of its similarity to natural convection between parallel plates (Rayleigh–Benard convection) and flow between rotating cylinders (Taylor–Couette flow). It has been determined [8–10] that fully developed flow between the plates does not alter the critical Rayleigh numbers of 1708, above which thermal instability results in the formation of longitudinal rolls aligned in the streamwise direction. Furthermore, the fully developed secondary flow causes the Nusselt number to be substantially larger than that for pure conduction ($Ra < 1708$). Heat transfer enhancement increases with Rayleigh number, but is independent of Reynolds number, indicating that, despite the bulk flow, heat transfer for fully developed conditions is essentially the same as that for pure natural convection. A breakdown in the laminar vortex structure was observed to occur at $Ra \approx 8000$.

Subsequent studies for the thermal entry region between isothermal parallel plates [11, 12] revealed that heat transfer was initially characterized by laminar forced convection and a steady decline in the

NOMENCLATURE

A	aspect ratio, W/H
g	acceleration due to gravity
Gr	Grashof number, $g\beta\Delta TH^3/\nu^2$
Gr^*	modified Grashof number, $g\beta qH^4/k\nu^2$
h	local heat transfer coefficient
H	height of channel or distance between plates
k	thermal conductivity
L	channel length
Nu	local Nusselt number, hH/k
Pr	Prandtl number
q	heat flux
Ra	Rayleigh number, $Gr\ Pr$
Ra^*	modified Rayleigh number, $Gr^*\ Pr$
Re	Reynolds number, $\bar{w}H/\nu$
T	temperature
W	width of channel
$\bar{w}$	average longitudinal velocity
z	longitudinal coordinate
z^*	inverse Graetz number, $z/H\ Re\ Pr$.

Greek symbols

β	coefficient of thermal expansion
ε	emissivity
θ	inclination angle from horizontal
ν	kinematic viscosity
σ	Stefan–Boltzmann constant.

Subscripts

b	local bulk condition
c	critical value (at onset of instability)
in	inlet condition
f	pure forced convection
s	bottom surface condition
t	top plate condition
z	based on longitudinal coordinate.

Nusselt number. Deviation from forced convection behavior corresponded to onset of the secondary flow, beyond which the Nusselt number approached an asymptotic value. With increasing Rayleigh number, the onset point moved upstream and the fully developed value of the Nusselt number increased.

In an experimental study of laminar water flow between horizontal parallel plates [13], top plate heating was found to be characterized by laminar forced convection and to have a negligible effect on mixed convection conditions at the bottom plate. In an extension of this study [14], flow visualization and local temperature measurements on the surface of a thin foil heater at the bottom of a parallel plate channel revealed conditions similar to those obtained for flow over a flat plate [3, 4]. An initial laminar forced convection region concluded with plumes rising from the heater surface and a sharp increase in the Nusselt number. The ensuing laminar mixed convection region was followed by plume oscillations which eventually yielded buoyancy driven turbulence.

Although mixed convection flow and heat transfer in rectangular channels have been predicted numerically [15, 16], such efforts are limited by the inability to obtain convergent solutions at large Rayleigh numbers and the inability to predict transition to turbulence. Furthermore, such solutions are typically for small aspect ratios, where sidewall effects are likely to be significant and parallel plate conditions are not well approximated. In one study, however, calculations were performed for aspect ratios up to 10 and longitudinal oscillations in the Nusselt number were predicted for the laminar mixed convection region [16].

While past research has contributed much to the understanding of mixed convection, unanswered questions remain, particularly for inclined channels which have yet to be considered experimentally. Issues requiring further study include the effects of heat flux, flow rate and inclination angle on mixed convection heat transfer both upstream and downstream of the onset of thermal instability. This paper reports on an experimental study of mixed convection heat transfer in a horizontal and inclined parallel plate channel which is uniformly heated from below.

2. EXPERIMENTAL APPARATUS AND PROCEDURES

2.1. *Apparatus*

Experiments were performed using the system shown schematically in Fig. 1. A regenerative blower is used to draw air through the flow conditioner and test section, with the flowrate controlled by the speed of the blower and a series of valves. The flowrate is measured to an accuracy of $\pm 1\%$ by one of two turbine flowmeters. Flexible hosing and two damping chambers isolate the test section acoustically and mechanically from the blower. A layer of open cell foam, a section of plastic honeycomb and a series of four fiberglass screens serve as a flow conditioner by filtering the incoming air, creating a uniform velocity profile, and reducing the intensity of ambient disturbances that enter the channel. The nozzle provides a two-dimensional contraction ratio of 31 : 1 and has been designed to eliminate flow separation, minimize turbulence, provide a nearly uniform velocity profile at the test section inlet, and to minimize the boundary layer thickness [17]. Boundary layer growth was analyzed numerically and found to be less than 10% of the channel height for $Re > 1500$. For $Re < 500$, however, boundary layer growth on the nozzle sur-

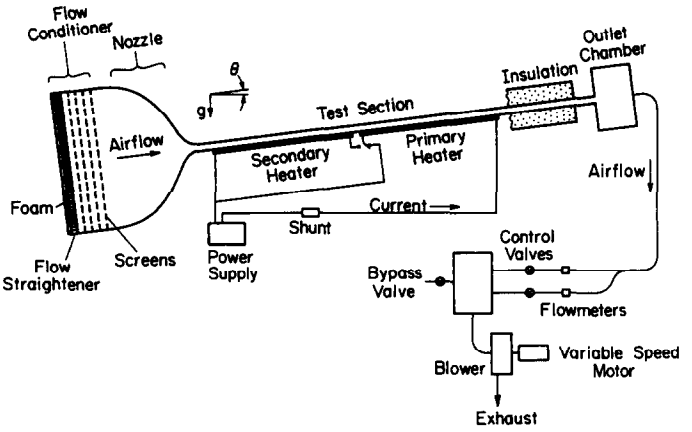

FIG. 1. Schematic of experimental apparatus.

faces resulted in appreciable velocity profile development prior to the channel inlet. This prediction was confirmed by velocity profile measurements made with a hot wire anemometer. Hence, in this channel, it is not possible to study simultaneous thermal and hydrodynamic boundary layer development at small Reynolds numbers.

The test section is constructed of acrylic top and side walls, with a height and width of $H = 30.5$ mm and $W = 308$ mm, providing an aspect ratio of $A \approx 10$ and a total length of $L = 2.4$ m. The bottom surface consists of two interchangeable heater plates, which could be heated independently or collectively. Assembly of the apparatus required a 33 mm unheated section between the two heaters. In most cases, only the downstream (primary) heater plate was used. Since the velocity profile develops over the length of the upstream unheated plate and is fully developed at the start of the second heater for $Re < 500$, this option allows for the study of thermal entry region conditions. Fully developed, laminar flow was verified at the leading edge of the primary heater plate through hot wire anemometry for $Re = 250$. By applying the prescribed heat flux to both plates, fully developed thermal conditions could be achieved on the downstream portion of the primary heater plate. Although the corresponding inlet velocity profile is neither uniform nor fully developed and may affect the onset of instability, it has little influence on the eventual fully developed condition. The entire channel was insulated with 0.25 m of styrofoam and fiberglass insulation and mounted on a rigid supporting frame which could be inclined up to 30° from the horizontal, creating a buoyancy assisted flow.

Each heater consists of a single sheet of 0.05 mm 321 stainless steel foil, 308 mm wide by 881 mm long. The uniformity of the foil was carefully checked, and double sided adhesive was used to bond the foil to a sheet of 3.2 mm masonite. Electric current was provided from a 40 V–60 A d.c. power supply and transferred to the foil through copper busbars firmly attached at both ends of the heater. Power dissipation was determined by measuring the current and voltage drop across the foil, and uniformity of the energy dissipation was checked by measuring the voltage distribution on the foil. Longitudinal measurements yielded a linear voltage drop, and spanwise measurements resolved variations no larger than 2 mV for a voltage drop of 2.3 V across the foil. The foil resistance was measured as a function of temperature and was found to increase by only 4.3% over the range from 30 to 70°C. For any test, the corresponding nonuniformity in the local heat dissipation was concluded to be less than $\pm 1.5\%$.

In order to ensure adequate resolution of longitudinal spanwise temperature distributions, the primary heater plate was instrumented with 160 36-gauge copper–constantan thermocouples which were carefully calibrated in order to resolve temperature differences as small as 0.02°C on the heater surface and 0.10°C between the heater and inlet air. Temperature measurements were concentrated near the midline of the heater, where edge effects are less significant, and toward the inlet, where conditions are expected to change more rapidly. The thermocouples were inserted through holes drilled in the insulation and masonite substrate and pushed gently against the adhesive, which isolated the junctions from the foil. Error in the temperature measurement caused by heat conduction in the thermocouple wire and across the foil/adhesive layer was predicted to be less than 0.5%. Additional thermocouples were used to measure temperatures of the inlet and outlet air, on the secondary heater, on the top plate, and to determine temperature differences across the insulation underneath the primary heater plate.

2.2. *Data reduction*

The Nusselt number

$$Nu = \frac{hH}{k} = \frac{q_{\text{conv}} H}{(T_s - T_b)k} \tag{1}$$

is obtained from measurement of the local surface temperature, calculation of the bulk temperature from an energy balance on the air, and calculation of the

local convective heat flux from a surface energy balance. The surface energy balance relates the total energy dissipated per unit area at any point on the surface to heat fluxes associated with convection, radiation and conduction

$$q_{tot} = q_{conv} + q_{rad} + q_{insul} + q_{long} + q_{span} \quad (2)$$

where conduction includes heat loss through the insulation, as well as a longitudinal and spanwise redistribution due to transfer in the foil and substrate materials. The convective heat flux is therefore determined by measuring the total dissipated flux and applying appropriate corrections for the nonconvective components of the heat flux. An implication of this expression is that, although uniform heat generation is achieved, variations in the radiation and conduction losses induce nonuniformities in the convective heat flux. The variations were less than approximately 20% for the conditions of this study, with the largest contribution coming from radiation exchange between the foil heater and the top acrylic surface.

Due to the large emissivity of the acrylic (0.83), the small emissivity (and correspondingly large uncertainty) of the stainless steel foil (0.10 ± 0.03), and the small separation between the plates, net radiation transfer from points near the centerline of the foil is satisfactorily approximated by the expression for radiation transfer between infinite isothermal plates

$$q_{rad} = \frac{\sigma(T_s^4 - T_t^4)}{1/\varepsilon_s + 1/\varepsilon_t - 1}. \quad (3)$$

With the foil temperature T_s measured directly and the top plate temperature T_t obtained by interpolation between measured values, radiation losses were estimated to range from 7 to 21% of the total flux, with an uncertainty in the calculation of approximately $\pm 30\%$.

Conduction losses through the insulation, q_{insul}, were calculated by assuming one-dimensional transfer and measuring the temperature difference across the first 50 mm of insulation beneath the foil heater. Losses calculated in this manner were less than 8% of the total, with an estimated uncertainty of approximately 10%.

Because the effect of longitudinal conduction in the foil and substrate could not be determined experimentally, attempts were made to assess its impact numerically by performing a two-dimensional conjugate analysis of flow in the channel and heat transfer by conduction in the foil and insulation. Employing standard finite-difference techniques [18], uniform heat generation was simulated by source terms in nodes representing the foil heater. Free convection losses from the bottom of the insulation were considered, while all other exterior boundaries were assumed adiabatic and radiation in the channel was neglected. Constant properties were assumed, along with the existence of laminar, forced convection in a

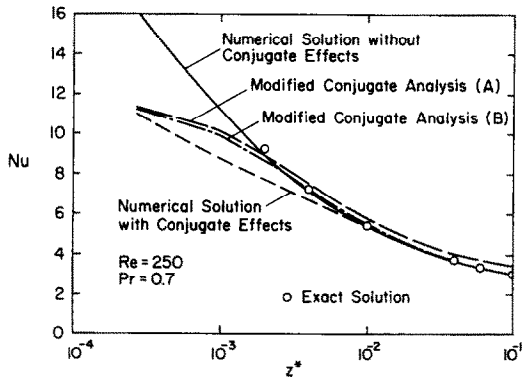

FIG. 2. Numerically determined Nusselt number distributions for two-dimensional forced convection.

thermal entry region. Although the assumption of forced convection is inconsistent with experimental conditions, for which there is onset of a buoyancy driven secondary flow, the onset point follows much of the decay in the convective coefficient which characterizes the thermal entry region. Hence the model is appropriate for upstream regions of the channel, where conduction effects are expected to be most pronounced and buoyancy effects are negligible.

The model predicts the surface temperature distribution, from which the local Nusselt number is determined. As shown in Fig. 2 results obtained for negligible conduction are in good agreement with the exact solution [19], thereby validating the numerical procedure. The lowermost curve in Fig. 2 corresponds to the fully conjugated numerical solution. The significant reduction in the Nusselt number is due to several effects which include: (i) the increase in upstream surface temperatures, and hence in the thermal boundary layer thickness, due to conduction from hotter downstream regions, (ii) conduction losses through the insulation, and (iii) to a lesser extent, the nonlinear increase in fluid bulk temperature due to redistribution of the heat flux. Note, however, that such effects are only important near the entrance and become negligible in downstream regions, where the Nusselt number approaches the exact solution.

To appreciate the extent to which conjugate effects influence the experimentally determined Nusselt number, the solution was used to generate the two remaining Nusselt number distributions of Fig. 2. In both cases the Nusselt number was based on the surface temperature obtained from the conjugate analysis. In case A, however, the convective flux used in calculating the Nusselt number was assumed equal to the flux dissipated in the foil heater, while in case B this flux was corrected for losses based on the assumption of one-dimensional conduction through the insulation. The case B result is analogous to the experimental distribution, for which the measured surface temperature is influenced by longitudinal conduction effects and the heat flux is corrected for losses. Hence, without correcting for the longitudinal conduction component of the generated heat flux, the measured

Nusselt number falls below the unconjugated forced convection limit near the inlet but closely approaches this limit in downstream regions (for $Re = 250$, case B is within 2% of the limit beyond the location of the third thermocouple at $z = 20$ mm, or $z^* = 3.8 \times 10^{-3}$). Since it is not possible to correct the measured results for longitudinal conduction in the foil and the insulation, the case B distribution should be considered the baseline with which data in the laminar forced convection region must agree.

Through a second analysis which considered spanwise conduction in the heater plate, it was determined that, although conjugate effects slightly distort the temperature distribution imposed by a three-dimensional secondary flow, they have an insignificant effect on the spanwise-averaged Nusselt number. Spanwise conduction was therefore neglected in calculating the longitudinal Nusselt number distribution.

The data reduction procedure accounted for fluid property variations, the nonlinear increase in bulk temperature due to varying losses, and flow acceleration caused by boundary layer growth and blockage at the side walls. By carefully accounting for all heat transfer processes, closure of an overall energy balance was achieved to within 5% for all test conditions. Moreover, the uncertainty in the Nusselt number was typically less than $\pm 10\%$, with exceptions corresponding to the highest heat fluxes, for which the radiation correction was important, and the lowest heat fluxes, for which temperature differences were very small.

After start-up, channel conditions were carefully maintained and monitored until steady state was achieved, generally after 6–10 h. Subsequent data acquisition and reduction were performed with a Hewlett–Packard 3054A data acquisition system and a 9826 computer.

3. RESULTS

3.1. *Horizontal orientation*

In Fig. 3 a typical spanwise-averaged longitudinal Nusselt number distribution is compared to the forced convection baseline for laminar flow between horizontal plates. The modified Grashof number ($Gr^* = 2.1 \times 10^5$) is based on the generated flux and the inlet conditions. Although losses make this number somewhat larger than the actual average Grashof number on the plate, this value consistently identifies the experiments and provides a basis for comparing similar test conditions. In Fig. 3(a), the sharp decay of the Nusselt number in the forced convection thermal entry region is stretched longitudinally through use of a logarithmic coordinate. However, since this study is primarily concerned with downstream conditions in the mixed convection regions, the results are more effectively displayed by the linear scale of Fig. 3(b). The monotonic decay in the Nusselt number associated with the laminar forced convection region ends when buoyancy forces become strong enough to destabilize the boundary layer. Beyond onset of the instability, plumes of warm fluid rise from the heated surface in a developing secondary flow, and plate temperatures are reduced by cool fluid descending from the core of the channel. This circulation provides a strong mechanism for heat transfer enhancement, and as the secondary flow strengthens, the Nusselt number rises well above the forced convection limit. In Fig. 3(b), enhancement achieves a maximum of approximately 100% before the Nusselt number begins to decay slightly. Beyond the maximum, fluid in the core has been warmed by the secondary flow and the descending fluid is no longer at the inlet temperature. With an increase in the temperature of the descending fluid, the reduction in the surface temperature is less pronounced and the Nusselt number begins to decay.

The foregoing trends were also revealed by the heat transfer measurements of Imura *et al.* [4] for flow over an isothermal flat plate and Knox and Incropera [14] for flow in a channel heated uniformly from below. The trends have also been numerically predicted by Incropera and Schutt [16]. The absence of longitudinal oscillations in the results of Kamotani and co-workers [11, 12] for channel flow may be partially due to the length of the heater segments over which local heat transfer measurements were averaged. The inability of Osborne and Incropera [13] to detect such variations has been attributed to significant plate conduction, which reduced large longitudinal temperature gradients [14]. By effectively eliminating plate conduction, Knox and Incropera were able to detect longitudinal Nusselt number oscillations.

The expected spanwise surface temperature variations caused by the three-dimensional nature of the secondary flow were verified by the measurements of this study. Spanwise Nusselt number distributions were uniform prior to the onset of instability, but significant variations ($\pm 15\%$) occurred after formation of the secondary flow. While interpretation of this distribution was limited by spanwise conduction and the large spacing between thermocouples (10 mm), the increase in the Nusselt number following thermal instability was always accompanied by spanwise variations. Changes in the Nusselt number with longitudinal distance, however, are well represented by the spanwise average.

By computing the standard deviation of plate temperatures averaged over a 10 min interval, some time-dependent behavior was noted for regions corresponding to heat transfer enhancement. In particular, the standard deviation increased sharply for locations downstream of the onset of instability, and the increase is attributed to unsteadiness of the secondary flow. These results agree with those of previous studies [3, 14], which observed varying degrees of unsteadiness for mixed convection.

3.1.1. *Effect of Grashof number.* Figure 4 depicts the spanwise averaged longitudinal Nusselt number distribution for $Re = 250$ and Grashof numbers in the range $1.0 \times 10^5 < Gr^* < 1.0 \times 10^6$. The distribution

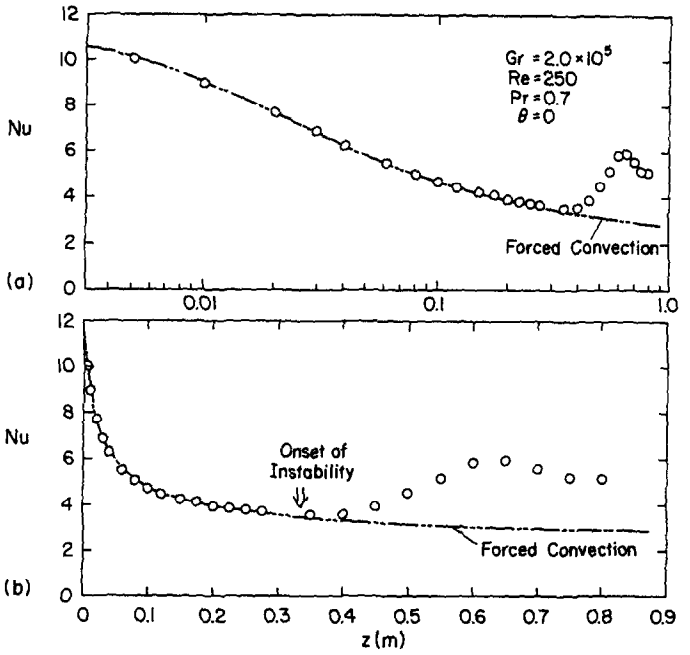

FIG. 3. Typical spanwise-averaged longitudinal Nusselt number distribution plotted on (a) log scale and (b) linear scale.

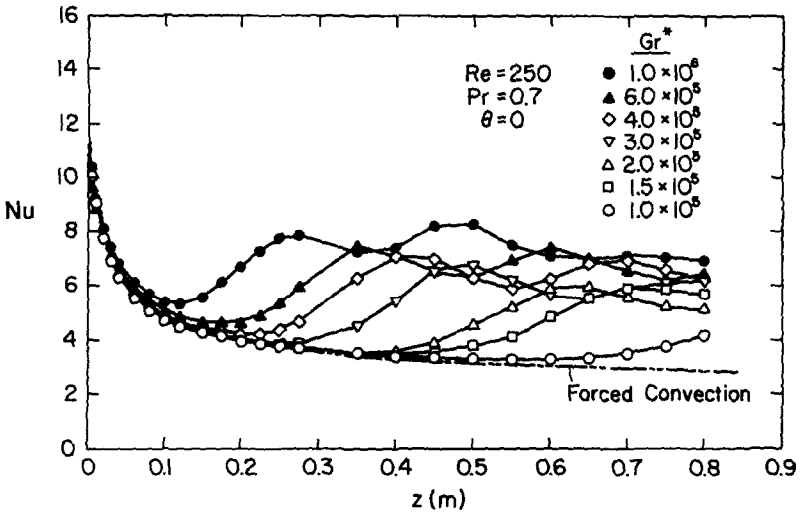

FIG. 4. Effect of modified Grashof number on longitudinal Nusselt number distribution.

for each modified Grashof number initially follows the forced convection limit. However, the location at which enhancement begins advances upstream with increasing Gr^*. This effect is due to increases in the thermal boundary layer thickness and the boundary layer temperature difference which accompany an increase in the surface heat flux and accelerate development of the secondary flow.

For the larger Grashof numbers, there is a discernible departure from the forced convection limit before a minimum in the Nusselt number is reached. Rapid boundary layer growth in this upstream region prevents the secondary flow from fully compensating for the effect of the thickening boundary layer. Hence, the Nusselt number, although enhanced above the forced convection limit, continues to decline. An additional contribution to heat transfer enhancement in this region may come from an induced streamwise pressure gradient. This effect in a channel heated uniformly from below has not been studied, and whether it can cause noticeable enhancement prior to thermal instability is not clear.

3.1.2. *Effect of Reynolds number.* Figure 5(a) demonstrates that one effect of an increase in the Reynolds number is to shift the onset of instability downstream. This observation and the channel geometry suggest that mixed convection flows may be scaled with the inverse Graetz number, $z^* = z/H\ Re\ Pr$. Although

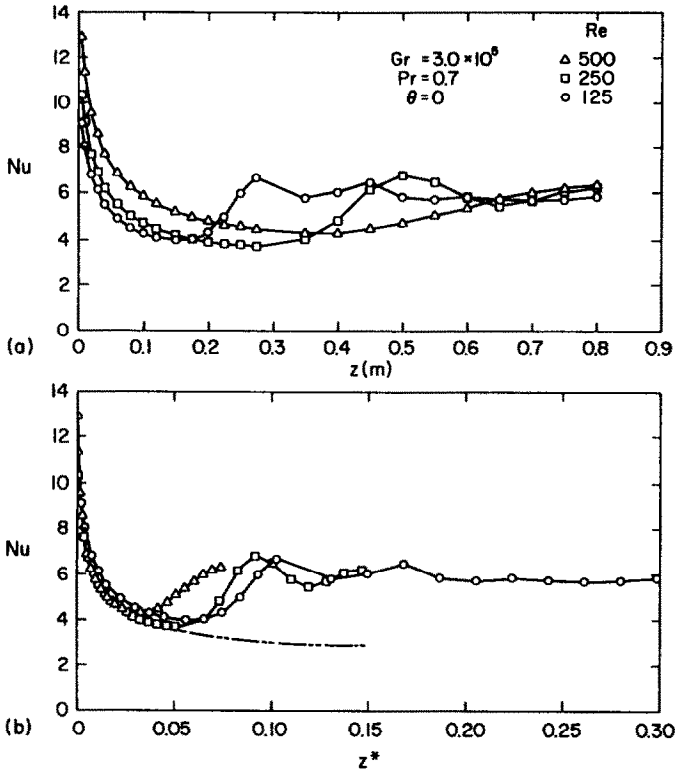

FIG. 5. Effect of Reynolds number on variation of Nusselt number with (a) the longitudinal coordinate and (b) the inverse Graetz number.

use of the parameter in Fig. 5(b) indicates reasonable scaling in the laminar forced convection region (except for $Re = 125$ where the streamwise pressure gradient may be important), the onset of instability and attendant heat transfer enhancement do not collapse entirely with z^*.

The governing equations may be nondimensionalized in terms of z^*, and Hwang and Cheng [20] have shown analytically that, for $Re\ Pr > 60$, fluid axial conduction is negligible and the onset of instability scales with z^*. Numerical predictions (which do not account for axial conduction) also suggest such scaling [16]. Experimental results [11, 12, 14, 21], however, show considerable scatter when plotted against the inverse Graetz number. Although this scatter may be at least partially caused by experimental uncertainties and property variations, existing experimental results do not confirm the suitability of z^* as a mixed convection scaling parameter.

3.1.3. *Fully developed conditions.* The data of Fig. 5(b) for $Re = 125$ suggest that initial oscillations in the Nusselt number decay to a final fully developed value. To further investigate the existence of fully developed conditions, uniform heat generation was maintained in both the upstream and downstream heater plates, providing a heated test section nearly 2 m long ($z/H = 59$). Plate temperature distributions measured for various Grashof numbers are shown in Fig. 6(a). At the channel inlet, there is a sharp initial temperature increase due to forced convection boundary layer growth. Plate cooling due to the secondary flow is also discernible for the larger Grashof numbers. Although the distance between the last thermocouple on the upstream plate and the first thermocouple on the second plate is 125 mm, the actual unheated length is only 33 mm. This interruption in heating causes partial cooling and mixing of the air by disrupting the thermal boundary layer. The renewed thermal boundary layer development occurring at the leading edge of the second plate is clearly revealed in Fig. 6(a), although renewed development is shortly followed by an approximately linear increase in temperature with increasing z. To determine if fully developed conditions had been achieved, the data were converted to the Nusselt number distributions shown in Fig. 6(b). The Nusselt number for each heat flux appears to approach a final asymptotic value, supporting the existence of a fully developed condition.

The data for $Gr^* = 7.0 \times 10^3$ are of particular interest. The heat flux for this case is very small (2 W m^{-2}), with a temperature difference of about 1°C between the plate surface and the local bulk fluid temperature. The Rayleigh number based on this temperature difference is approximately 1200, which is lower than the value of 1708 required for instability in a fully developed flow. Although the data are influenced by the interrupted heating and errors associated with the small temperature difference, it does not appear that the fully developed Nusselt number is enhanced above the forced convection limit of 2.69.

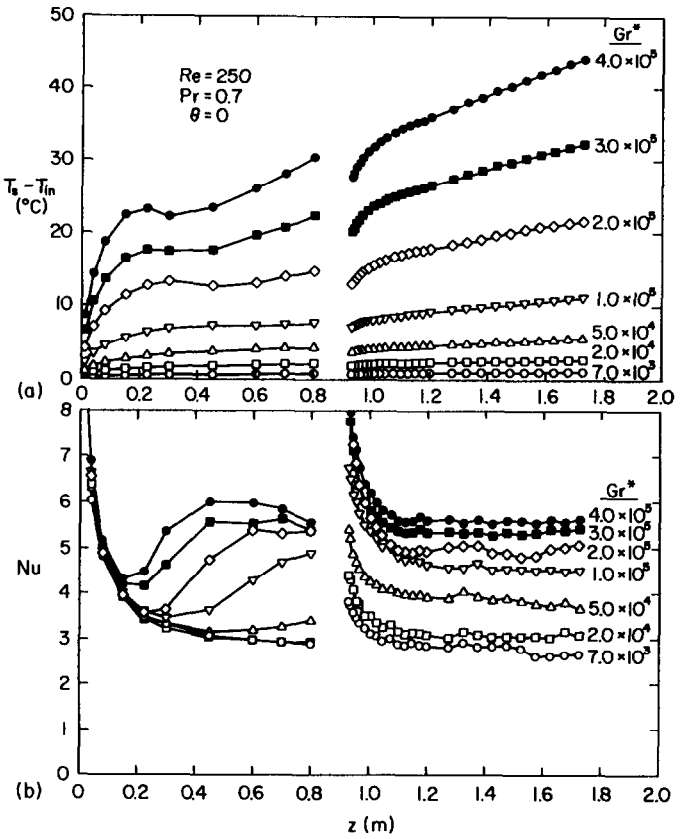

FIG. 6. Longitudinal distributions of (a) plate temperature and (b) Nusselt number for channel with both heater plates active.

The foregoing result is more clearly seen in Fig. 7, where the fully developed Nusselt number for each experiment is plotted against the Rayleigh number based on the temperature difference. For the smallest Rayleigh number, the Nusselt number is approximately equal to the forced convection limit, while larger Rayleigh numbers provide enhancement above this value. At the larger Rayleigh numbers, the data are well correlated by $Ra^{1/3}$. The exponent of 1/3 indicates that the heat transfer coefficient is independent of the length scale, which is characteristic of turbulent free convection. Flow visualization in water [14] has confirmed that laminar mixed convection can undergo transition to turbulence at large Rayleigh numbers. Further evidence for the existence of a turbulent end state was provided by the spanwise temperature distributions obtained for the larger Rayleigh numbers. While measurements just beyond the onset of instability showed large spanwise variations, spanwise distributions in the fully developed region were nearly uniform.

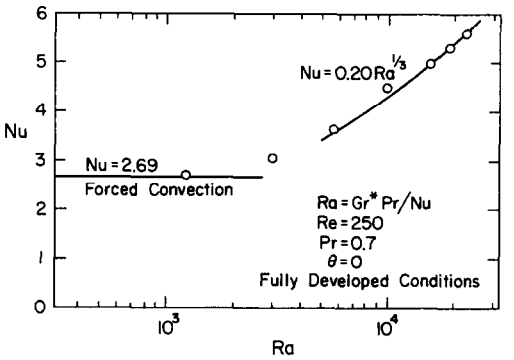

FIG. 7. Effect of Rayleigh number on fully developed Nusselt number.

3.2. *Inclined orientation*

In an inclined channel, the buoyancy force is no longer exclusively perpendicular to the heated surface, since a component also exists in the streamwise direction. The effect of this component on the local Nusselt number is seen in Fig. 8, where data for $Re = 250$, $0 < \theta < 30°$, and five different Grashof numbers ($1.0 \times 10^5 < Gr^* < 6.0 \times 10^5$) are plotted. The buoyancy force in the direction of flow ($g \sin \theta$) accelerates the fluid in the thermal boundary layer and increases the heat transfer coefficient well before the onset of instability. In Fig. 8(d), for example, the Nusselt number for the horizontal plate ($\theta = 0$) still corresponds to laminar forced convection at a longitudinal distance of 20 cm. Data for $\theta = 20°$, however, are 10% higher, while at $\theta = 30°$, enhancement has increased to 15%. A comparison with Fig. 8(a) ($Gr^* = 1.0 \times 10^5$) shows that flow acceleration and

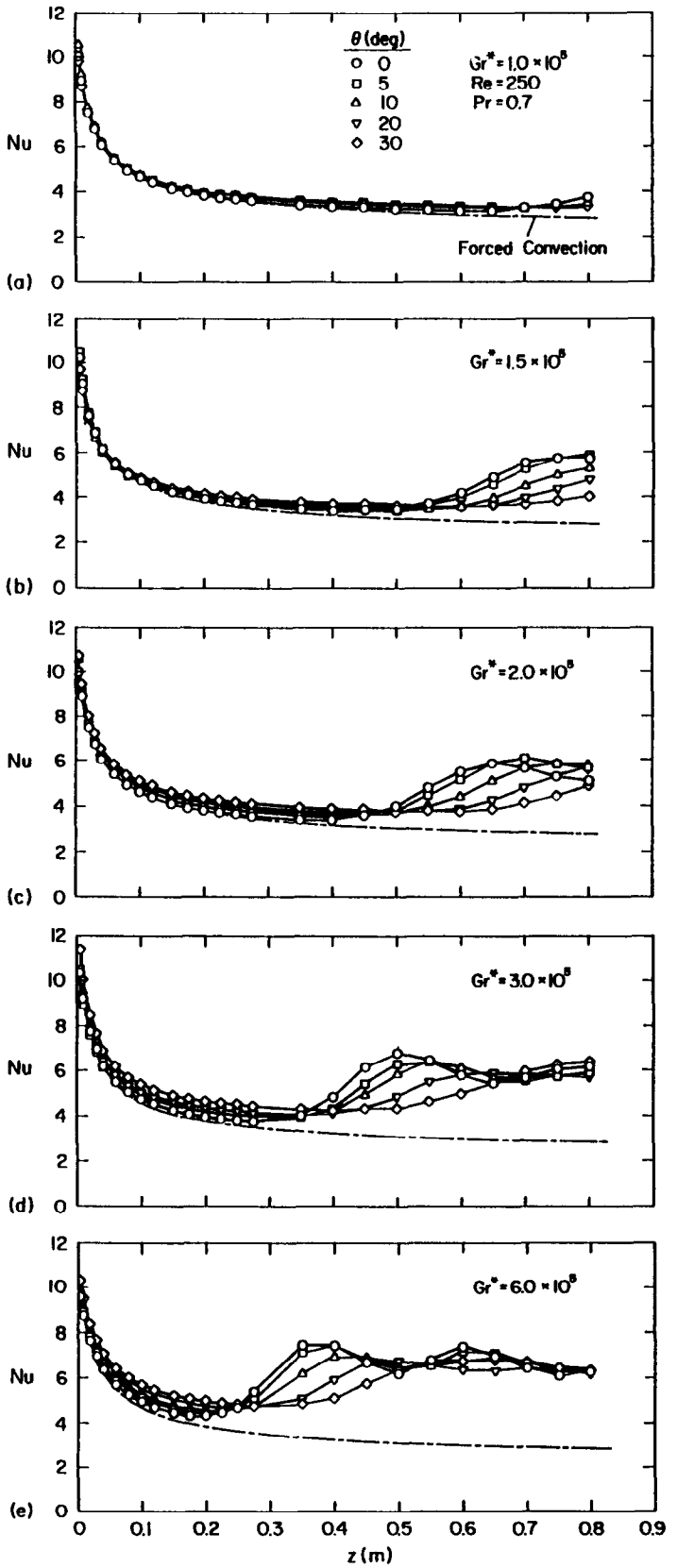

FIG. 8. Effect of inclination angle on longitudinal Nusselt number distribution for $Re = 250$ and $Pr = 0.7$: (a) $Gr^* = 10^5$, (b) $Gr^* = 1.5 \times 10^5$, (c) $Gr^* = 2 \times 10^5$, (d) $Gr^* = 3 \times 10^5$, (e) $Gr^* = 6 \times 10^5$.

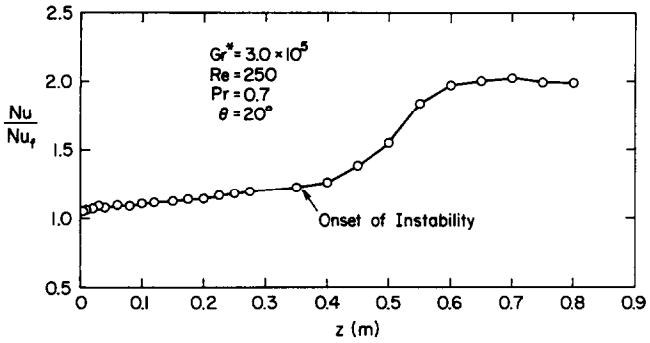

FIG. 9. Identification of onset of instability from longitudinal distribution of heat transfer enhancement.

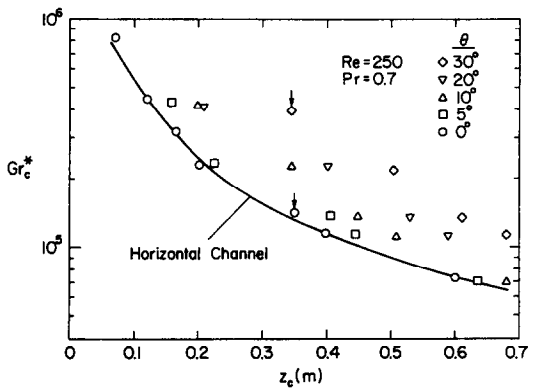

FIG. 10. Onset of instability for airflow in a parallel plate channel heated from below.

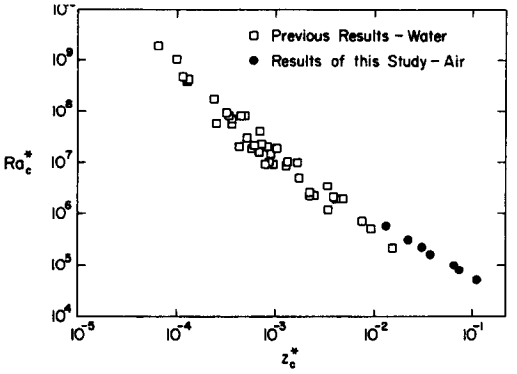

FIG. 11. Comparison of instability data with previous results for water in a horizontal channel heated from below.

the corresponding heat transfer enhancement increase with the heat flux, as well as with the inclination angle. Although Ramanchandran *et al.* [6] were able to correlate two-dimensional heat transfer enhancement on an inclined flat plate in terms of the parameter $Gr_z \sin\theta/Re_z$, similar attempts to correlate the channel data of this study were unsuccessful.

Fluid acceleration also delays the onset of instability by decreasing the boundary layer thickness (Fig. 8(c)). In addition stability increases with inclination due to the decreasing component of the cross-stream buoyancy force ($g \cos\theta$).

3.3. *Onset of instability*

Although it is common to associate onset of thermal instability with the first longitudinal station at which heat transfer enhancement is discernible, this criterion is inappropriate for inclined channels, since enhancement may be due to streamwise acceleration of the flow upstream of the onset point. Hence, for this study, the onset point was inferred from enhancement curves, such as that of Fig. 9. Near the onset point, enhancement begins to deviate sharply from a gradual increase with the longitudinal coordinate. The gradual increase is attributed to streamwise acceleration of fluid in the boundary layer, and the subsequent sharp increase is attributed to development of the secondary flow. For each experiment, the onset of instability was determined (approximately) in the foregoing manner, and results are plotted in Fig. 10. The critical Grashof number is based on the average of actual plate conditions upstream of the onset point, rather than on inlet conditions. Previously reported trends are evident in the figure. Namely, the thermal instability advances with increasing heat flux and moves downstream with increasing inclination angle. The stabilizing effect of streamwise acceleration is noteworthy. For example, with $Gr^* = 4.6 \times 10^5$ and $\theta = 30°$, instability occurs at the same location as in a horizontal channel with less than half the heat flux, or $Gr^* = 2.1 \times 10^5$. Since the cross-stream gravitational component decreases by only 15% as the channel is tilted by 30°, this large difference is attributable to the increased streamwise velocity. For this reason attempts to correlate the data with $g \cos\theta$ have been unsuccessful.

In Fig. 11 data for the horizontal channel are compared to previous results for water flow in channels heated uniformly from below [14]. The comparison, which is made in terms of the modified Rayleigh number, suggests that air is slightly more stable than water. These results may also be compared to previous data for airflow in channels. Since the earlier experiments involved flow visualization between isothermal plates, the modified Rayleigh numbers of this study have been converted to Rayleigh numbers based on a suitable temperature difference. In accordance with the appropriate definitions, this conversion was performed by dividing the modified Rayleigh number by the average Nusselt number upstream from the onset

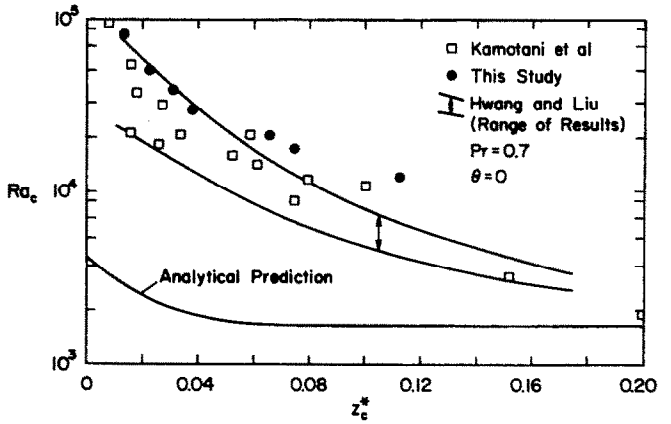

FIG. 12. Comparison of instability data with previous results for airflow between horizontal isothermal plates.

of instability, thereby prescribing the bulk temperature as the reference temperature. The characteristic length remains the channel height. As shown in Fig. 12, the results of this study suggest delayed onset of instability for uniform heating. This result may be due to the small temperature differences on the upstream portion of a plate which is uniformly heated. The theoretical results of Hwang and Cheng [20] are also noted on the figure. The large discrepancy is attributed to the large distance over which a disturbance must amplify before it can have a perceptible influence on the boundary layer.

4. SUMMARY

Surface temperature measurements in a parallel plate channel heated uniformly from below were corrected for radiation and insulation losses and converted to longitudinal distributions of the Nusselt number. Such distributions showed a rapid decline in the thermal entry region that agreed well with numerical predictions based on a forced convection, conjugate analysis. Subsequent heat transfer enhancement was attributed to the formation and development of a buoyancy driven secondary flow. Experiments revealed that longitudinal oscillations in the Nusselt number corresponding to secondary flow development subsequently decayed to a fully developed value that depended on the Grashof number. Large heat flux data were well correlated by the Rayleigh number to the one third power, indicating that the fully developed condition is characteristic of turbulent free convection.

The onset of instability was found to move upstream for increasing Grashof number and to be delayed for an increasing Reynolds number. Inclining the channel for buoyancy-assisted flow resulted in appreciable heat transfer enhancement prior to the onset of instability, as well as a significant delay in formation of the secondary flow. Attempts to correlate the data in terms of $g \cos \theta$ and z^* were not successful.

Acknowledgements—Support of this work by the National Science Foundation under Grant No. CBT-8316580 is gratefully acknowledged. One of the authors (J.R.M.) is also grateful for fellowships provided by the Chevron Corporation and the NL Industries Foundation.

REFERENCES

1. Y. Mori, Buoyancy effects in forced laminar convection flow over a horizontal flat plate, *J. Heat Transfer* **83,** 479–482 (1961).
2. E. M. Sparrow and W. J. Minkowycz, Buoyancy effects on horizontal boundary layer flow and heat transfer, *Int. J. Heat Mass Transfer* **5,** 505–511 (1962).
3. R. R. Gilpin, H. Imura and K. C. Cheng, Experiments on the onset of longitudinal vortices in horizontal Blasius flow heated from below, *J. Heat Transfer* **100,** 71–77 (1978).
4. H. Imura, R. R. Gilpin and K. C. Cheng, An experimental investigation of heat transfer and buoyancy induced transition from laminar forced convection to turbulent free convection over a horizontal isothermally heated plate, *J. Heat Transfer* **100,** 429–434 (1978).
5. A. Mucoglu and T. S. Chen, Mixed convection on inclined surfaces, *J. Heat Transfer* **101,** 422–426 (1979).
6. N. Ramanchandran, B. F. Armaly and T. S. Chen, *Measurements of Laminar Mixed Convection Flows Adjacent to an Inclined Surface* (Edited by B. F. Armaly and L. S. Yao), ASME HTD-Vol. 53, pp. 45–50 (1985).
7. T. S. Chen, A. Moutsoglou and B. F. Armaly, Thermal instability of mixed convection flow over an inclined surface, *Numer. Heat Transfer* **5,** 343–352 (1982).
8. A. Pellew and R. V. Southwell, On maintained convection motion in a fluid heated from below, *Proc. R. Soc.* **A176,** 312–343 (1940).
9. Y. Mori and Y. Uchida, Forced convection heat transfer between horizontal flat plates, *Int. J. Heat Mass Transfer* **9,** 803–816 (1966).
10. S. Ostrach and Y. Kamotani, Heat transfer augmentation in laminar fully developed channel flow by means of heating from below, *J. Heat Transfer* **97,** 220–225 (1975).
11. Y. Kamotani and S. Ostrach, Effect of thermal instability on thermally developing laminar channel flow, *J. Heat Transfer* **98,** 62–66 (1976).
12. Y. Kamotani, S. Ostrach and H. Miao, Convective heat transfer augmentation in thermal entrance regions by means of thermal instability, *J. Heat Transfer* **101,** 222–226 (1979).
13. D. G. Osborne and F. P. Incropera, Laminar mixed

convection heat transfer for flow between horizontal parallel plates with asymmetric heating, *Int. J. Heat Mass Transfer* **28,** 207–217 (1985).
14. A. L. Knox and F. P. Incropera, Mixed convection flow and heat transfer in the entry region of a horizontal rectangular duct, ASME paper 86-HT-18 (1986).
15. K. C. Cheng and J. W. Ou, Convective instability and finite amplitude convection in the thermal entrance region of horizontal rectangular channels heated from below, *Proc. 7th Int. Heat Transfer Conf.* **2,** 189–194 (1982).
16. F. P. Incropera and J. A. Schutt, Numerical simulation of laminar mixed convection in the entrance region of horizontal rectangular ducts, *Numer. Heat Transfer* **8,** 707–729 (1985).
17. T. Morel, Design of two-dimensional wind tunnel contractions, *J. Fluids Engng* **99,** 371–378 (1971).
18. S. V. Patankar, *Numerical Heat Transfer and Fluid Flow.* Hemisphere, Washington, D.C. (1980).
19. R. E. Lundberg, W. C. Reynolds and W. M. Kays, Heat transfer with laminar flow in concentric annuli with constant and variable wall temperature and heat flux, NASA TN-D-1975 (1963).
20. G. J. Hwang and K. C. Cheng, Convective instability in the thermal entrance region of a horizontal parallel plate channel heated from below, *J. Heat Transfer* **95,** 72–77 (1973).
21. G. J. Hwang and C. L. Liu, An experimental study of convective instability in the thermal entrance region of a horizontal parallel plate channel heated from below, *Can. J. Chem. Engng* **54,** 521–525 (1976).

EXPERIENCES SUR LA CONVECTION THERMIQUE MIXTE POUR UN ECOULEMENT D'AIR DANS UN CANAL HORIZONTAL OU INCLINE

Résumé—Des expériences on été faites sur la convection mixte de la chaleur dans la région d'entrée d'un canal plat chauffé uniformément par le bas. L'effet du flux thermique et l'orientation du canal sur le nombre local de Nusselt est étudié pour $Pr = 0{,}7$, $125 < Re < 500$, $7 \cdot 10^3 < Gr^* < 10^6$ et $0 < \theta < 30°$. Le transfert thermique est initialement dominé par la convection forcée et il montre un déclin rapide en nombre de Nusselt. A la suite de l'apparition de l'instabilité thermique, un développement d'écoulement secondaire cause une forte augmentation du nombre de Nusselt qui est suivie d'un maximum et d'oscillations. Ces oscillations du nombre de Nusselt diminuent éventuellement jusqu'à une valeur pleinement établie qui dépend du nombre de Grashof. L'apparition de l'instabilité est retardée par la diminution du nombre de Grashof et/ou par l'augmentation du nombre de Reynolds et de l'angle d'inclinaison. Pour le canal incliné, un accroissement significatif du transfert thermique se produit avant l'apparition de l'écoulement secondaire.

EXPERIMENTELLE BESTIMMUNG DES WÄRMEÜBERGANGS AN EINEN LUFTSTROM BEI MISCHKONVEKTION IN EINEM HORIZONTALEN UND GENEIGTEN KANAL

Zusammenfassung—Die Experimente wurden durchgeführt, um den Wärmeübergang bei Mischkonvektion im Einlaufbereich einer Spaltströmung bei aufgeprägter Wärmestromdichte an der unteren Platte zu untersuchen. Es wurde der Einfluß der Wärmestromdichte und der Kanalneigung auf die örtliche Nusselt-Zahl für $Pr = 0{,}7$; $125 < Re < 500$; $7 \cdot 10^3 < Gr < 10^6$ und $0 < \theta < 30°$ untersucht. Der Wärmeübergang wurde zu Beginn hauptsächlich durch die erzwungene Konvektion bestimmt und zeigte ein schnelles Abnehmen der Nusselt-Zahl. Nach Einsetzen der thermischen Instabilität verursachte das Auftreten einer Sekundärströmung ein starkes Ansteigen der Nusselt-Zahl bis zu einem Maximum mit nachfolgenden Schwingungen. Die Schwingungen klingen möglicherweise bis auf einen konstanten Wert ab, der eine Funktion der Grashof-Zahl ist. Das Eintreten der Instabilität wird durch Verringerung der Grashof-Zahl und/oder durch Erhöhung der Reynolds-Zahl und des Neigungswinkels verzögert. Beim geneigten Kanal trat die signifikante Erhöhung des Wärmeübergangs bereits vor dem Einsetzen der Sekundärströmung auf.

ЭКСПЕРИМЕНТАЛЬНОЕ ИССЛЕДОВАНИЕ ТЕПЛООБМЕНА ПРИ СМЕШАННОЙ КОНВЕКЦИИ ВОЗДУХА В ГОРИЗОНТАЛЬНОМ И НАКЛОННОМ КАНАЛАХ

Аннотация—Проведены эксперименты по изучению смешанного конвективного теплопереноса в тепловой входной области плоскопараллельного канала, равномерно нагреваемого снизу. Изучалось влияние плотности теплового потока и ориентации канала на местное число Нуссельта для $Pr = 0{,}7$ и $125 < Re < 500$, $7 \cdot 10^3 < Gr < 1 \cdot 10^6$ и $0 < \theta < 30°$. Первоначально преобладающий вклад в теплообмен вносила вынужденная конвекция, что приводило к резкому уменьшению числа Нуссельта. После возникновения тепловой неустойчивости развивались вторичные течения, которые вызывали резкий рост числа Нуссельта, сменяющийся после достижения максимума периодическими колебаниями. Далее колебания числа Нуссельта полностью прекращались и достигалась величина, зависящая от числа Грасгофа. Начало возникновения неустойчивости можно затянуть, уменьшая число Грасгофа и/или увеличивая число Рейнольдса и угол наклона. Для наклонного канала наблюдалось значительное усиление теплообмена еще до начала вторичного течения.